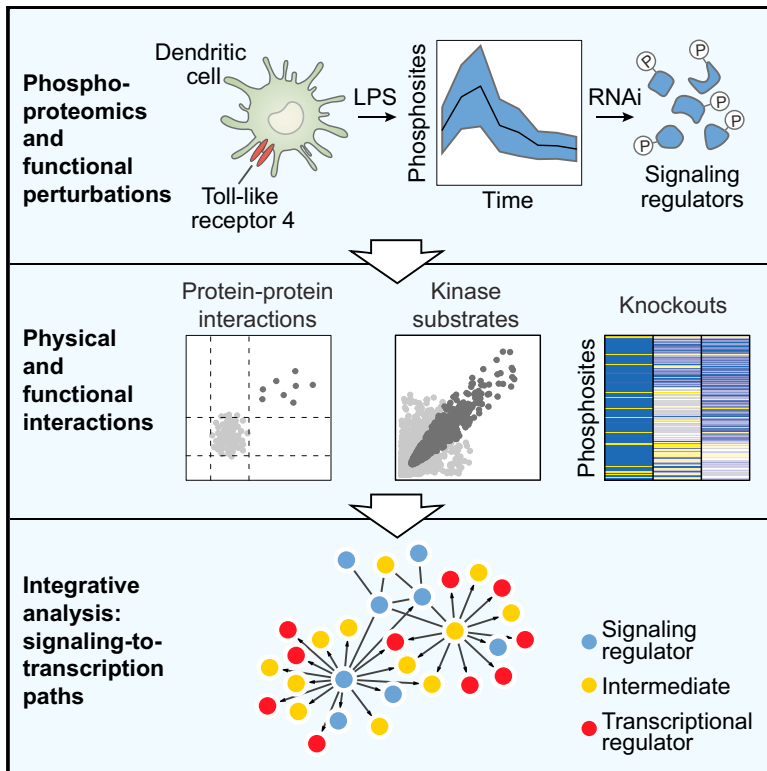# An Integrative Framework Reveals Signaling-to-Transcription Events in Toll-like Receptor Signaling

Graphical Abstract

Authors

Philipp Mertins, Dariusz Przybylski, Nir Yosef, ..., Aviv Regev, Nir Hacohen, Nicolas Chevrier

Correspondence

aregev@broadinstitute.org (A.R.), nhacohen@mgh.harvard.edu (N.H.), chevrier@fas.harvard.edu (N.C.)

In Brief

Mertins et al. develop a systematic framework to unify the study of signaling and transcriptional regulatory networks. By integrating physical, enzymatic, and functional interaction data, they identify biochemical paths that connect Toll-like receptor (TLR) 4 signaling to transcription. Their analysis uncovers two dozen regulators in TLR signaling, including AP1AR and PICALM, which link vesicle transport to pro-inflammatory responses.

Highlights

- Temporal analysis of phosphorylation networks in LPS-treated dendritic cells (DCs)

- AP1AR and its binding partner, PICALM, as pro-inflammatory signaling regulators

- Biochemical framework to dissect physical, enzymatic, and functional interactions

- Integrative modeling of signaling-to-transcriptional paths downstream of TLR4

CellPress

An Integrative Framework Reveals
Signaling-to-Transcription Events
in Toll-like Receptor Signaling

Philipp Mertins,[1,7] Dariusz Przybylski,[1,7] Nir Yosef,[1,2] Jana Qiao,[1] Karl Clauser,[1] Raktima Raychowdhury,[1]
Thomas M. Eisenhaure,[1] Tanja Maritzen,[3] Volker Haucke,[3] Takashi Satoh,[4] Shizuo Akira,[4] Steven A. Carr,[1] Aviv Regev,[1,5,*]
Nir Hacohen,[1,6,*] and Nicolas Chevrier[1,8,9,*]
[1]Broad Institute of MIT and Harvard, 415 Main Street, Cambridge, MA 02142, USA
[2]Department of Electrical Engineering and Computer Science and Center for Computational Biology, University of California, Berkeley,
Berkeley, CA 94720, USA
[3]Molecular Physiology and Cell Biology Section, Leibniz-Institute for Molecular Pharmacology (FMP), 13125 Berlin, Germany
[4]WPI Immunology Frontier Research Center, Osaka University, 3-1 Yamada-oka, Suita, Osaka 565-0871, Japan
[5]Howard Hughes Medical Institute, Department of Biology, MIT, Cambridge, MA 02142, USA
[6]Center for Immunology and Inflammatory Diseases and Center for Cancer Research, Massachusetts General Hospital, Charlestown, MA
02129, USA
[7]These authors contributed equally
[8]Present address: FAS Center for Systems Biology, Harvard University, Cambridge, MA 02138, USA
[9]Lead Contact
*Correspondence: aregev@broadinstitute.org (A.R.), nhacohen@mgh.harvard.edu (N.H.), chevrier@fas.harvard.edu (N.C.)
http://dx.doi.org/10.1016/j.celrep.2017.06.016

SUMMARY

Building an integrated view of cellular responses to
environmental cues remains a fundamental chal-
lenge due to the complexity of intracellular networks
in mammalian cells. Here, we introduce an integra-
tive biochemical and genetic framework to dissect
signal transduction events using multiple data types
and, in particular, to unify signaling and transcrip-
tional networks. Using the Toll-like receptor (TLR)
system as a model cellular response, we generate
multifaceted datasets on physical, enzymatic, and
functional interactions and integrate these data to
reveal biochemical paths that connect TLR4
signaling to transcription. We define the roles of
proximal TLR4 kinases, identify and functionally
test two dozen candidate regulators, and demon-
strate a role for *Ap1ar* (encoding the Gadkin protein)
and its binding partner, *Picalm*, potentially linking
vesicle transport with pro-inflammatory responses.
Our study thus demonstrates how deciphering dy-
namic cellular responses by integrating datasets on
various regulatory layers defines key components
and higher-order logic underlying signaling-to-tran-
scription pathways.

INTRODUCTION

Signaling networks must coordinate multiple layers of regulation
throughout the cell to respond to environmental changes. For

example, mammalian immune cells detect microbial molecules
thanks to pathogen-sensing pathways such as Toll-like recep-
tors (TLRs) (Takeuchi and Akira, 2010). Upon activation by their
cognate ligands, TLRs follow general principles of signal trans-
duction by recruiting cytosolic adaptors and downstream en-
zymes such as kinases, which triggers cascades of biochemical
changes leading to cellular outputs such as gene expression
changes (Figures 1A and 1B). A fundamental question in cellular
response systems, such as TLRs, is how to generate and
combine knowledge about signaling and transcription regulatory
networks to build an integrated view of the flow of information in
a cell. Answering this question will help close gaps in our knowl-
edge of intracellular wiring and inform therapeutic targeting of
cellular components that are central to disease.

Despite recent advances in measuring cellular processes
and associated biochemical changes from many different angles
(e.g., post-translational modifications, gene expression, and
transcription factor binding), building integrated models of
signaling pathways that take into account multiple regulatory
layers remains an elusive task due to several challenges. First,
using prior knowledge from databases alone, it is hard to
compare and connect signaling nodes and processes that
have been studied in disparate systems and with different read-
outs. Furthermore, existing databases are largely incomplete, as
demonstrated by the fact that the vast majority of known phos-
phorylation sites remain orphans with respect to their matching
kinases. Second, acquiring data within a single cellular context
and across regulatory processes ranging from post-translational
modifications (PTMs) to protein complexes to kinase substrates
is difficult due to the various technical requirements of each
assay, making them hard to adapt within a unique and relevant
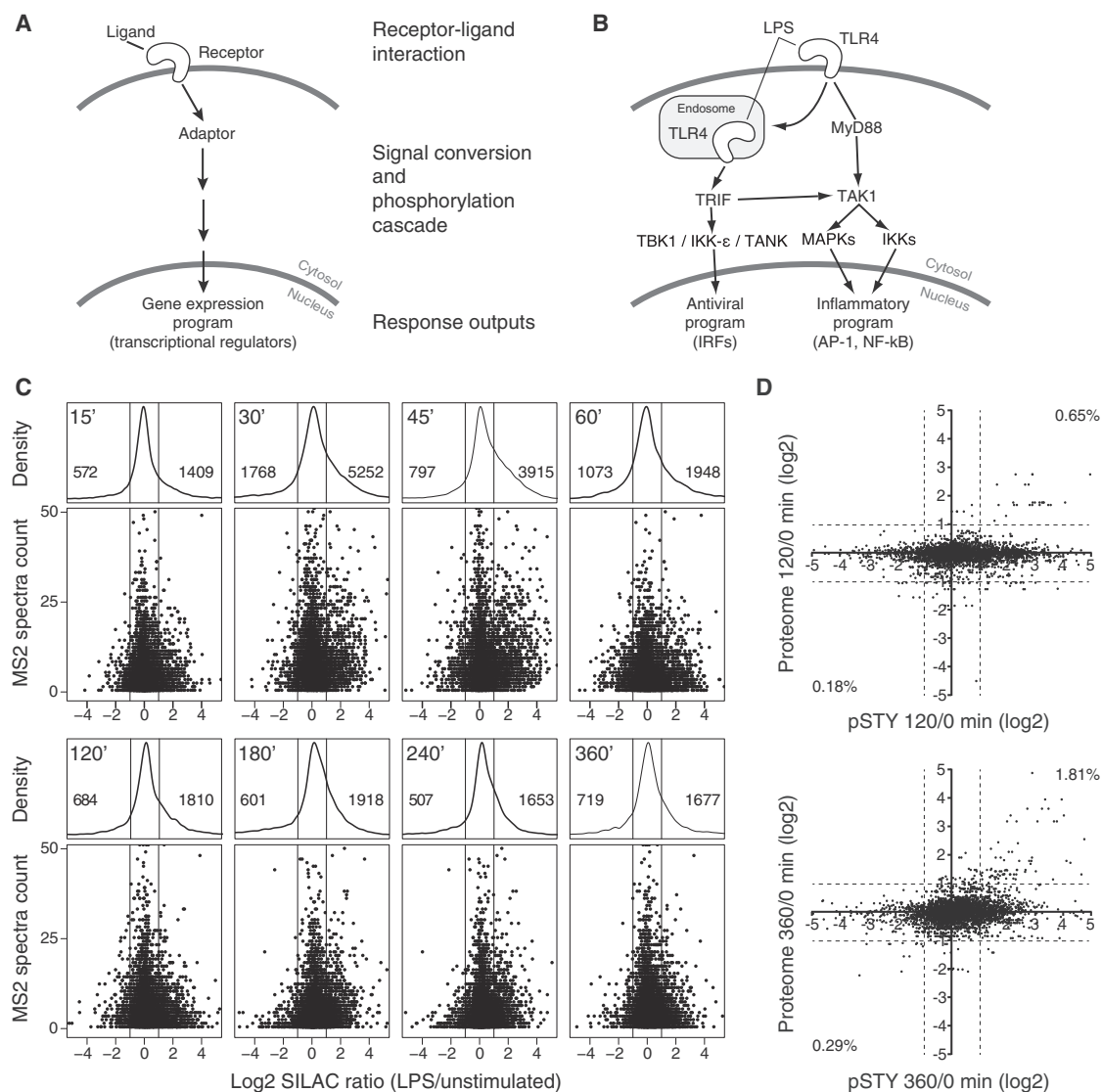cellular context. Third, individual large-scale measurements are

Figure 1. TLR4 Stimulation with LPS Leads to Global and Dynamic Changes in the Phosphoproteome of DCs

(A and B) Diagram highlighting general principles of cellular signaling-to-transcription events (A) and their transposition to the TLR4 pathway (B).

(C) Temporal changes in the phosphoproteome of LPS-stimulated DCs. Shown are the distributions of log2 fold changes of phosphosites (x axis) between LPS-treated and untreated cells at indicated times after LPS stimulation, as density (top of each panel) and dot plots (bottom of each panel, with MS2 spectra count in y axis and showing phosphosites measured in all eight time points).

(D) Comparison between the phosphoproteome and total proteome of LPS-stimulated DCs. Shown are distributions of log2 fold changes of phosphosites (x axis) and proteins (y axis) between LPS-treated and untreated cells at 120 (top) and 360 (bottom) min post-stimulation.

See also Figure S1 and Table S1.

inherently limited by their variability in sensitivity and specificity and are often used to capture static snapshots rather than the dynamic events of cellular responses. It is thus critical to address these challenges to help to dissect the connections that form the basis of multi-layered cellular responses (Bensimon et al., 2012; Santra et al., 2014; Yugi et al., 2016).

Here, we hypothesized that integrating measurements spanning, in the context of a single cellular response model, both signaling and transcriptional regulatory layers will help to reveal key network-wide properties that would otherwise not

be observable. To test this, building upon prior work (Chevrier et al., 2011), we developed an experimental and computational framework to measure and integrate the information underlying signaling-to-transcription events in the TLR system, from the membrane to gene regulation. We measure dynamic changes in two types of interactions: physical (i.e., phosphorylation, kinase-substrate relationships, protein-protein and DNA-protein interactions) and functional (i.e., effects of genetic perturbations on gene expression or phosphorylation events) (Figure S1A). Using these datasets, we identify regulators of TLR4 responses in

dendritic cells (DCs), including AP1AR and its binding partner, PICALM, and introduce a network-based computational approach that takes advantage of these diverse measurements to decipher the higher-order logic governing TLR signaling-to-transcription events.

RESULTS

The Dynamic Phosphoproteome of LPS-Stimulated Dendritic Cells

We reasoned that large-scale, dynamic measurements of the changes in protein phosphorylation in lipopolysaccharide (LPS)-treated DCs would help to reconstruct signaling-to-transcription pathways, because TLR signaling functions through phosphorylation of its own constituents, from kinases such as mitogen-activated protein kinases (MAPKs), IRAKs, IKKs, or TBK1 to transcription factors such as nuclear factor κB (NF-κB) or IRFs (Figure 1B) (Takeuchi and Akira, 2010). Furthermore, work by others (Sharma et al., 2010; Sjoelund et al., 2014; Weintz et al., 2010) and us (Chevrier et al., 2011) showed that phosphoproteomics can identify regulators of the TLR system. We used stable isotope labeling with amino acids in cell culture (SILAC)-based phosphoproteomics to compare the levels of phospho-serine, phospho-threonine, and phospho-tyrosine sites between DCs left untreated as control or stimulated with LPS at eight time points (15, 30, 45, 60, 120, 180, 240, and 360 min) (Figures S1B and S1C). We identified and quantified a total of 20,975 phosphosites derived from 5,789 distinct proteins in at least two LPS-stimulated samples (false discovery rate [FDR] < 1%; Figure 1C; Table S1), of which 20.5% were present in all eight time points (4,310/20,975 phosphosites from 1,952 proteins; Figure S1D) due to undersampling of highly complex and low-signal-intensity phosphopeptide mixtures in individual SILAC experiments. The largest changes in the DC phosphoproteome were observed at 30 and 45 min after LPS stimulation, which covered 92.8% of all quantified phosphosites in this study (19,456/20,795) (Figure S1E). In addition, these changes in phosphorylation were not due to changes in protein amounts, as only 0.65 and 1.81% of proteins showed an increase in both phosphorylation and protein levels at 2 and 6 hr after LPS stimulation, respectively (Figure 1D). These results suggested that LPS stimulation modifies a large fraction of the DC phosphoproteome within an hour.

Temporal Analysis of Phosphorylation Changes Highlights Known and Candidate Regulators of TLR4 Signaling

Next, to study the dynamics of the LPS-regulated phosphoproteome, we focused on the 3,557 phosphosites mapping onto 1,606 proteins that were quantified in at least six out of eight time points and differentially regulated upon LPS stimulation in a single or two consecutive time points (2,071/3,557 phosphosites for the latter) (Table S2). Overall, 53.4% (3,557/6,659) of the phosphosites quantified in at least six independent time points were found to be differentially regulated by LPS, which corresponds to 61.4% (1,606/2,617) at the phosphoprotein level. We used k-means clustering to partition these 3,557 phosphosites into ten co-abundance clusters with distinct temporal

profiles (Figures 2A and S2A). We found three general patterns of changes in phosphorylation levels: (1) early upregulation until 45 min (clusters I and II), (2) late upregulation after 120 min (cluster III), and (3) downregulation at various times (clusters IV–X) (Figure 2B). Each temporal cluster contained known TLR pathway proteins for a total of 43 out of 141 canonical TLR components, including 7.8% (11/141) and 10.6% (15/141) for clusters I and II, respectively (Figures 2B and S2B). Known TLR proteins identified in this data encompassed both positive (e.g., MAPK family, IRF3, and NF-κB) and negative (e.g., TANK and TNFAIP3) regulators, and were differentially phosphorylated at multiple sites in some cases (Figure S2C). The 1,606 phosphoproteins present in these ten temporal clusters were enriched for molecular functions, including kinases, transcriptional regulators, or protein binding (Figure S2D). Some of the enriched gene sets pointed to nascent areas of TLR biology, such as the organization and regulation of the TLR system within the framework of intracellular organelles and structures (e.g., activity and regulation of GTPases, cytoskeleton; Figure S2D). Cluster II, and to a lesser extent other clusters, showed a significant enrichment for other immune signaling pathways (e.g., B and T cell receptor signaling or DNA-sensing pathways), highlighting the existence of shared proteins between these immune response systems (Figure S2D). Taken together, these results reveal the dynamic changes imparted on the DC phosphoproteome by LPS, which include known and putative regulators of TLR4 signaling as well as processes linked to DC biology, such as changes in cell shape, motility, metabolism, and antigen processing.

Genetic Perturbations of Phosphorylated Proteins Identify Putative Regulators of TLR4 Signaling

To test if the phosphoproteins identified above play a role in the TLR system, we used our temporal and enrichment analyses to prioritize candidates for genetic perturbations (Figure 3A). We focused on 751 phosphoproteins from the 1,606 ones used for temporal clustering, which were upregulated at 30 and 45 min after LPS treatment (clusters I and II; Figure 2B). We reasoned that using early clusters would help to identify candidate regulators likely to be downstream of TLR4 by avoiding feedbacks from transcription or autocrine and paracrine signaling. Third, we selected 169 out of 751 phosphoproteins to test by retaining all enzymes (e.g., kinases and GTPases) and enzyme binders and regulators (e.g., GTPase regulators) (Figures S3A and S3B; Table S3). All selected phosphoproteins were also found to be expressed at the mRNA level in DCs (Garber et al., 2012). The two TLR4 adaptor proteins MYD88 and TRIF (encoded by Ticam1) were part of these candidate genes. MYD88 was added manually as a positive control, although it was not found to be differentially phosphorylated, whereas TRIF matched our selection criteria above.

We successfully perturbed 131 out of 168 candidate genes with an average knockdown efficiency of 81% ± 9% SD (Figure S3C). We stimulated DCs with LPS and measured the effect of gene silencing on the mRNA levels of 263 TLR response signature genes, representing the inflammatory and antiviral programs (Table S3). We determined statistically significant changes in the expression of signature transcripts upon
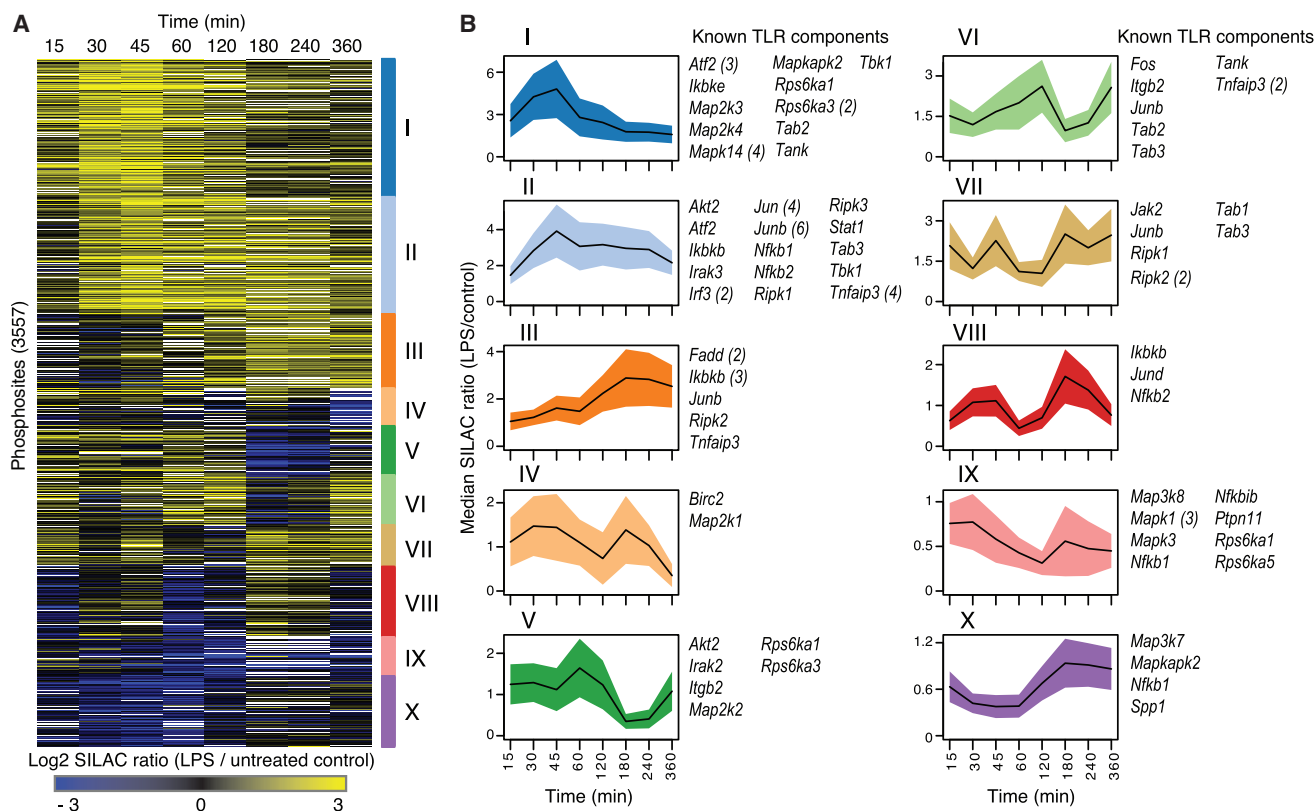
Figure 2. Temporal Analysis of the LPS-Induced Phosphoproteome Reveals Known and Candidate Regulators of TLR4 Signaling
(A) Temporal phosphorylation profiles during LPS stimulation in DCs. Log2 fold changes between LPS-treated and untreated cells for 3,557 phosphosites (rows) detected in at least six out of eight time points (columns). Phosphosites are partitioned into ten clusters using k-means (color bars, right). White indicates missing values.
(B) Median log2 fold changes between LPS-treated and untreated cells (y axis) and median absolute deviation (MAD; colored error bar) at each time point (x axis) for phosphosites in all ten k-means clusters from (A). Known TLR pathway proteins detected in each cluster are indicated on the right. Parentheses indicate the number of phosphosites per proteins (when >1).
See also Figure S2 and Table S2.

individual knockdowns based on comparisons to 16 control genes, whose expression remains unchanged upon TLR activation, and to 38 control short hairpin RNAs (shRNAs) that did not affect TLR signature genes. 27 out of the 131 genes tested significantly affected TLR signature gene expression, which included known TLR signaling components such as TICAM1, TBK1, MAPK9, RIPK3, and IRAK2 (Figure 3B). Furthermore, several phosphoproteins were reported to function in TLR signaling by independent studies: TRAFD1 (Sanada et al., 2008), STK3 (Geng et al., 2015), ULK1 (Eriksen et al., 2015), and CORO1A (Tanigawa et al., 2009). Interestingly, known and candidate components had similar effects on the TLR gene signature upon knockdown. By measuring the pairwise similarity among these 27 perturbation profiles (using Pearson's correlation), we observed three major modules of signaling regulators: MYD88 and a set of four proteins (SAMHD1, TBC1D17, AP1AR, and PDLIM7) affecting inflammatory gene expression (module I), TICAM1 and five proteins (module II), and 16 proteins displaying effects that overlap with MYD88 and/or TICAM1 (module III) (Figure 3B).

Validation of AP1AR and Other Candidate Regulators of the Myd88-Dependent Inflammatory Pathway
We next sought to validate the putative roles of the four phosphoproteins (AP1AR, PDLIM7, SAMHD1, and TBC1D17) whose perturbation profiles closely resembled that of MYD88 in controlling pro-inflammatory genes (Figure 4A). We measured the expression levels of inflammatory and antiviral cytokines in LPS-stimulated DCs infected by two independent, gene-specific lentiviral shRNAs per candidate phosphoprotein. We observed a decrease in inflammatory cytokine mRNA expression compared to eight control hairpins in all cases (Il6, Cxcl1, and, to a lesser extent, Tnf), whereas antiviral cytokines Ifit1 and Cxcl10 were mostly unaffected (Figure 4B). Similarly, using mouse $Ap1ar^{-/-}$ knockout DCs (Maritzen et al., 2012), we observed a strong decrease in inflammatory cytokines, especially Il1b, Il12b, and Tnf, whereas antiviral cytokines were not affected (Ifnb1) or slightly reduced (Cxcl10) (Figure 4C).
To generate mechanistic insights about the putative role of AP1AR in the TLR4 pathway, we sought to identify binding partners of AP1AR in LPS-stimulated DCs using affinity purification
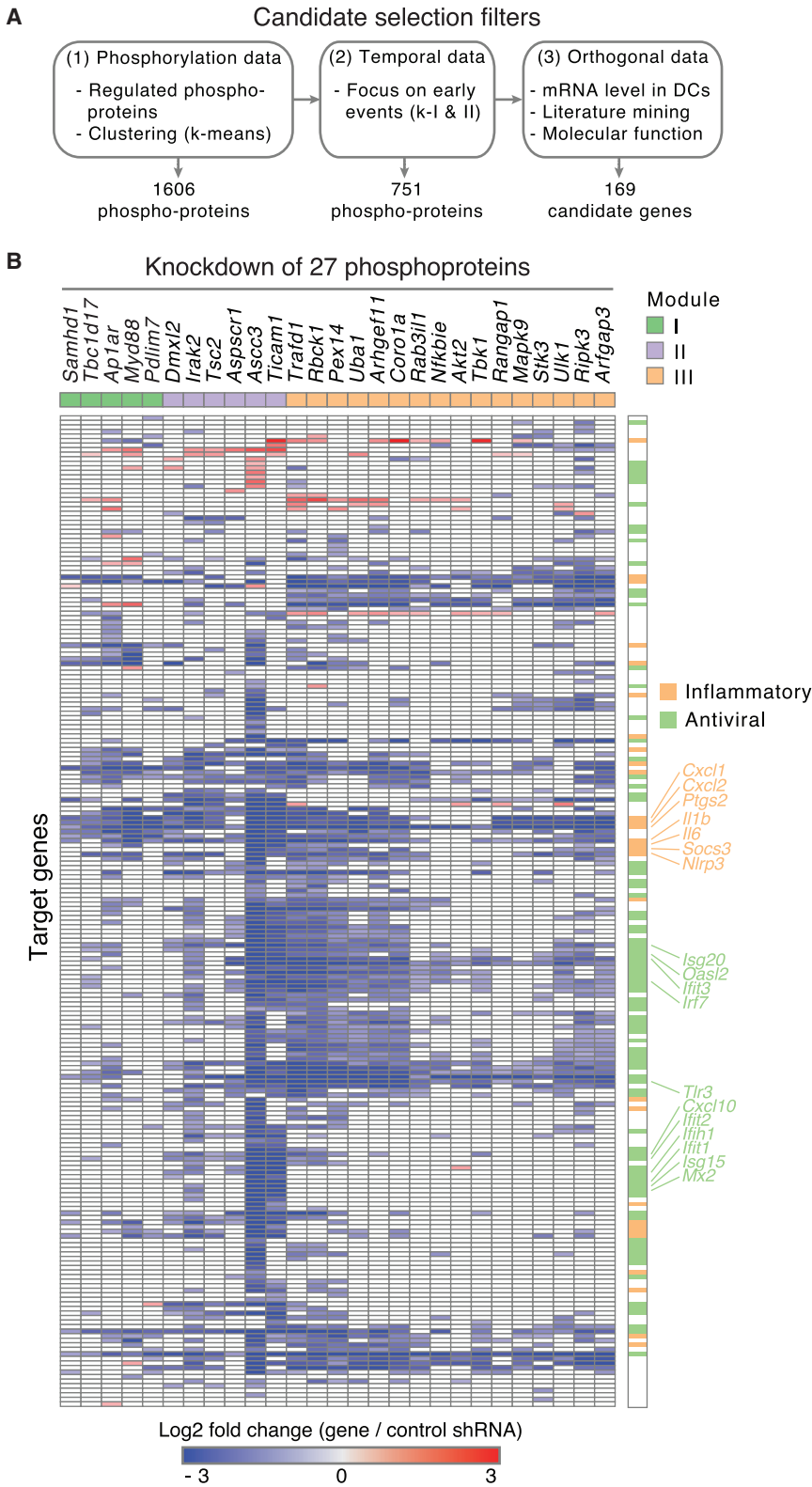
A

Candidate selection filters

(1) Phosphorylation data
- Regulated phospho-proteins
- Clustering (k-means)

→

(2) Temporal data
- Focus on early events (k-I & II)

→

(3) Orthogonal data
- mRNA level in DCs
- Literature mining
- Molecular function

↓
1606 phospho-proteins

↓
751 phospho-proteins

↓
169 candidate genes

B

Knockdown of 27 phosphoproteins

Columns: *Samhd1, Tbc1d17, Ap1ar, Myd88, Pdlim7, Dmxl2, Irak2, Tsc2, Aspscr1, Ascc3, Ticam1, Trafd1, Rbck1, Pex14, Uba1, Arhgef11, Coro1a, Rab3il1, Nfkbie, Akt2, Tbk1, Rangap1, Mapk9, Stk3, Ulk1, Ripk3, Arfgap3*

Module
- I (green)
- II (purple)
- III (orange)

Inflammatory (orange)
Antiviral (green)

Inflammatory genes: *Cxcl1, Cxcl2, Ptgs2, Il1b, Il6, Socs3, Nlrp3*

Antiviral genes: *Isg20, Oasl2, Ifit3, Irf7*

Tlr3, Cxcl10, Ifit2, Ifih1, Ifit1, Isg15, Mx2

Target genes

Log2 fold change (gene / control shRNA)

-3   0   3

Figure 3. Genetic Perturbations of Phosphorylated Proteins Identify Putative Regulators of TLR4 Signaling

(A) Overview of phosphoprotein candidate selection for functional analysis.

(B) Perturbation profiles of the 27 phosphoproteins that significantly impacted TLR4 outputs. Shown are the perturbed candidates and control phosphoproteins (columns) and the log2 fold changes for each target gene (rows) between gene-specific and control shRNAs. The rightmost column categorizes target genes into antiviral (light green) and inflammatory (light orange) programs.
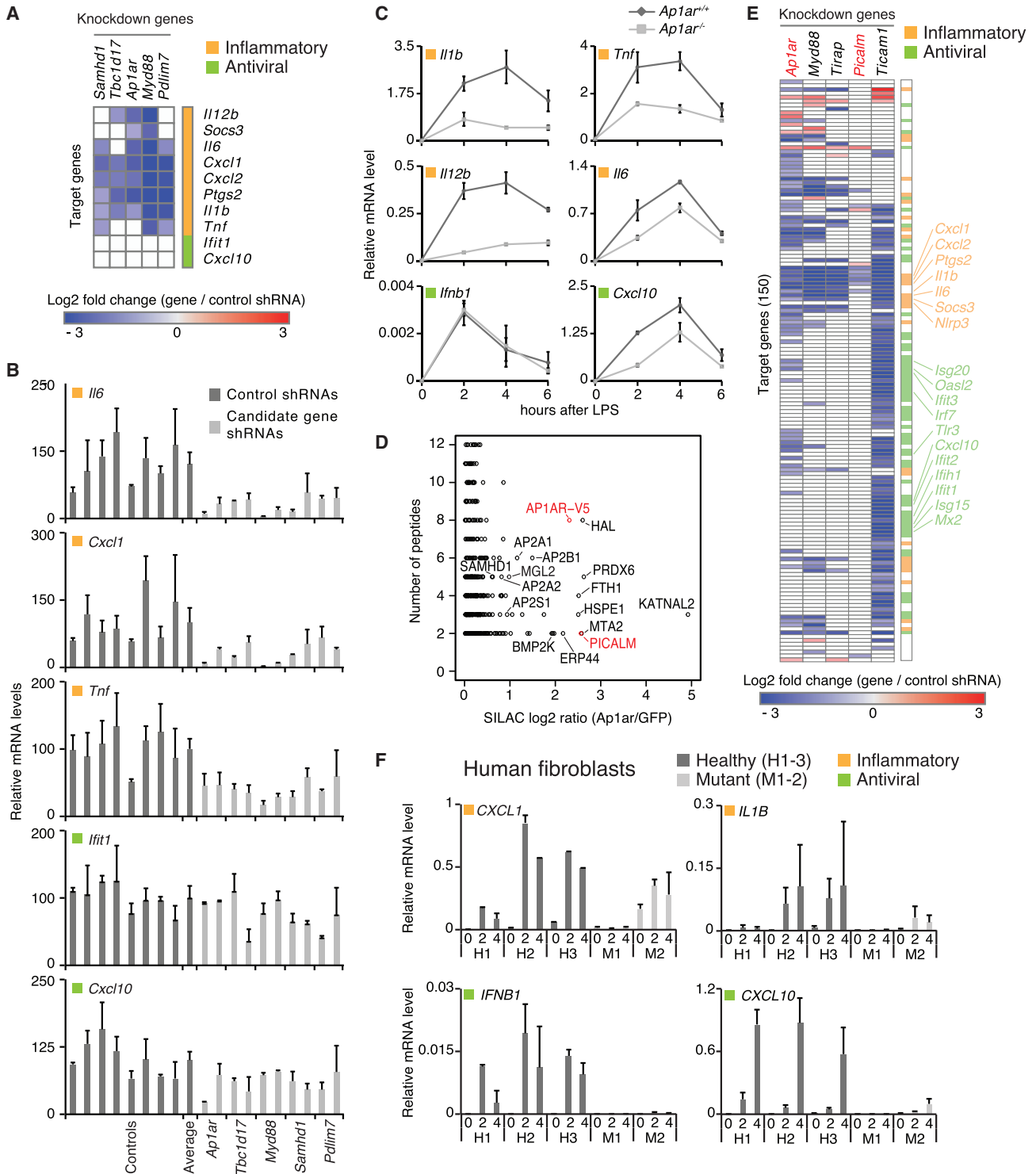
See also Figure S3 and Table S3.

Figure 4. Identification of Candidate Regulators in the MYD88-Dependent Inflammatory Pathway

(A) Perturbation profiles of genes affecting the MYD88 pathway. Shown are four perturbed candidate genes and MYD88 (columns) and the log2 fold changes between gene-specific and control shRNAs (rows) of ten target genes. The rightmost column categorizes target genes into antiviral (light green) and inflammatory (light orange) programs.

(B) Expression levels (qPCR) relative to control shRNAs (left bars, dark gray) for two antiviral cytokines (*Ifit1* and *Cxcl10*) and three inflammatory cytokines (*Il6*, *Cxcl1*, and *Tnf*) following LPS stimulation in DCs using two independent shRNAs. Bottom tick marks separate shRNAs controls and each gene (average indicates the mean value for all eight control shRNAs). Two to three replicates for each experiment; error bars represent SD.

(legend continued on next page)

followed by mass spectrometry in primary mouse DCs (Figure S4A). Protein overexpression was effective in nearly all transduced cells as measured by GFP fluorescence and did not impact cell responsiveness to LPS, as shown by strong morphological changes (Figure S4B). We overexpressed V5-tagged AP1AR and GFP as control bait in SILAC-labeled DCs stimulated with LPS for 30 min (Figure S4C), which led to the identification of proteins that co-precipitated with AP1AR, but not GFP (Figure 4D; Table S4). Several known components of the assembly protein complex 2 (AP-2) were pulled down with AP1AR (AP2A1, AP2B1, and AP2S1), as well as the AP-2 binding partner PICALM, which is an important component of clathrin-mediated endocytosis (Miller et al., 2015). Next, to test if some of these AP1AR binders affect TLR4 signaling outputs, we turned back to genetic perturbations followed by gene signature measurements. Out of ten putative AP1AR binders (at least two peptides identified and >1.5 log2 SILAC ratio of AP1AR/GFP), six showed a knockdown efficiency >50%. We found that PICALM led to a decrease in the induction of LPS-induced inflammatory genes similarly to MYD88, TIRAP, and AP1AR (Figure 4E). Altogether, these results suggest a potential mechanism whereby AP1AR and PICALM act together in the regulation of MYD88-dependent inflammatory signaling.

For another candidate identified based on phosphorylation changes, SAMHD1, we further tested its potential involvement in TLR signaling using human skin fibroblasts derived from Aicardi-Goutières syndrome (AGS) patients that carry deleterious SAMHD1 mutations (Crow and Manel, 2015). We observed a decrease in both inflammatory and antiviral gene expression upon LPS stimulation in two independent patient cell lines compared to three healthy controls (Figure 4F), which differed from knockout mouse DC data (Figure S4D). The latter observation might be attributable to the difference in cellular context or to compensatory mechanisms in the mouse knockout cells. Interestingly, physical interactions between SAMHD1 and TLR pathway proteins have been reported previously, such as the TLR4 adaptor protein TIRAP (Li et al., 2011), and also with CCNA2 and CDK2, which can be activated by TLR4 signaling (Hasan et al., 2007; Huttlin et al., 2015). Altogether, we gathered evidence supporting that AP1AR, its binding partner PICALM, and SAMHD1 are likely to act as regulators of pro-inflammatory TLR4 signaling.

Signaling Regulator Perturbation Profiles Overlap with Transcription Factor Target Genes, Suggesting Potential Signaling-to-Transcription Paths

Having shown that phosphorylation dynamics can help identify potential regulators of TLR signaling-to-transcription events, we next sought to identify how signaling regulators are connected to downstream transcriptional regulators. The two targeted screens for candidate (1) phosphoproteins and (2) AP1AR binders led to 29 perturbation profiles showing significant changes in TLR signature genes upon LPS stimulation (Figures 3B and 4E). Based on the similarity of these perturbation-induced expression profiles (Pearson's correlation), we partitioned these 29 proteins into three modules (Figure 5A; similar to Figure 3B). Next, we asked what transcription factors (TFs) are likely to act downstream of these three modules of proteins by taking advantage of existing data on the binding sites across the genome of 23 TFs involved in TLR4 signaling (Garber et al., 2012). We reasoned that measuring the overlaps between genes whose promoters are bound by a TF, and genes whose mRNA levels are impacted by knockdown of a phosphoprotein, would help to infer some of the signaling regulator-TF relationships likely to be active upon TLR4 activation (Figure S5). For 20 out of 23 TFs tested, we identified significant overlaps (p value < 0.05; hypergeometric test) between gene sets whose promoters were bound by one or several TFs and those whose mRNA levels were impacted by knockdown of 25 out of 29 candidate and known regulators (Figure 5B; Table S5). Some of these overlaps recapitulated known signaling regulator-TF relationships in the TLR pathways, such as MYD88 and NF-κB family members REL and RELB, or TRIF and IRFs and STATs. Gene targets of AP1AR, MYD88, and PICALM overlapped significantly with genes bound by RUNX1 and REL. Taken together, these results further support a role for the 29 phosphoproteins identified downstream of TLR4 and suggest the existence of signaling regulator-TF relationships between 25 phosphoproteins and 20 TFs.

Physical and Functional Proteomics Pinpoint Binding and Phosphorylation Events Downstream of the Myd88 Adaptor and Associate Kinases

Next, to decipher the biochemical events linking the signaling to transcriptional regulator relationships identified above, we measured protein-protein and kinase-substrate interactions by focusing on MYD88-dependent signaling. First, in DCs stimulated with LPS for 30 min, we rediscovered most known MYD88 binding partners, including TIRAP, TRAF6, or IRAK family kinases, which support the validity of our affinity-purification coupled with mass spectrometry (AP-MS) assay in primary DCs (Figures 6A and S6A; Table S6). IRAK2 immunoprecipitation identified several interaction partners such as MYD88 and TRAF6 but with lower enrichment ratios compared to MYD88, which is likely due to the short-lived interaction dynamics of kinases (Figure 6B).

(C) Inhibition of transcription of inflammation cytokines in *Ap1ar*$^{-/-}$ DCs. mRNA levels (qPCR; relative to Gapdh) for indicated inflammatory (light orange) and antiviral (light green) cytokines in three replicates per time point. Error bars represent SD.

(D) Interaction proteomics identified putative binders for AP1AR in DCs. Log2 fold change (x axis) of proteins enriched differentially between DCs expressing V5-tagged-AP1AR and -GFP (control bait) plotted against the number of peptides identified per protein (y axis).

(E) Perturbation profiles of indicated genes (columns) and the log2 fold changes between gene-specific and control shRNAs (rows) of 150 target genes. The rightmost column categorizes target genes into antiviral (light green) and inflammatory (light orange) programs.

(F) Impact of SAMHD1 mutations on human fibroblast cell response to LPS. Human fibroblasts from healthy (H) or mutant-carrying patients (M; with homozygous c.445C > T p.Gln149* for M1 and c.1609-1G > C for M2) were stimulated with LPS or left untreated as control, and indicated inflammatory (light orange) and antiviral (light green) cytokine levels were measured by qPCR (relative to GAPDH). Error bars represent SD.

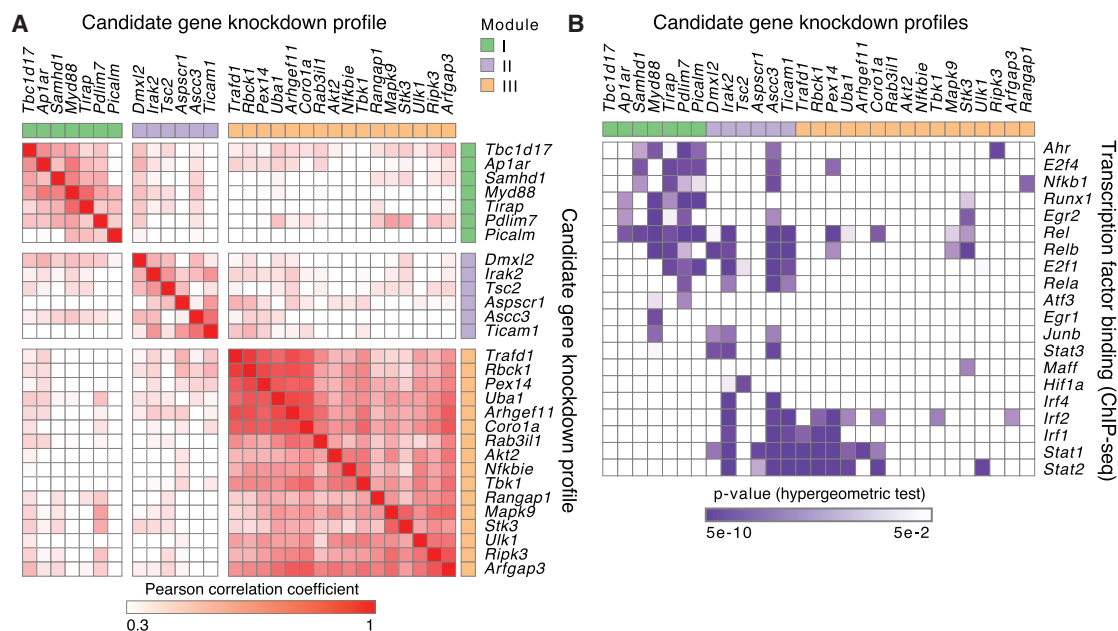See also Figure S4 and Table S4.

Figure 5. Similarities in Perturbation Profiles and Overlap with TF Target Genes Suggest Three Functional Modules for the 29 Candidate Phosphoproteins

(A) Functional classification based on similarity of perturbation profiles. Shown is a correlation matrix (Pearson correlation coefficient) of the perturbation profiles from Figures 3B and 4E combined.

(B) Intersection between genes affected by a phosphoprotein perturbation and genes whose promoters are bound by transcription factors (TFs). Shown are the overlaps between genes affected by 29 candidate signaling regulators knockdowns (columns, including positive control genes) and genes whose promoters are bound by 20 TFs (rows). P values, hypergeometric test (purple: significant correlation; white: no correlation).

See also Figure S5 and Table S5.

Second, we used two complementary approaches to identify the substrates downstream of MYD88-associated kinases, which remain poorly characterized. Perturbation approaches followed by phosphoproteomics have proven useful in determining functional pathway components downstream of a given network node (Bodenmiller et al., 2010; Chevrier et al., 2011). We measured the impact of four knockout (KO) models ($Myd88^{-/-}$, $Myd88^{-/-}/Ticam1^{-/-}$, which abrogates all TLR4 signals), $Irak2^{-/-}$ and $Irak4^{-/-}$) on the DC phosphoproteome upon LPS stimulation for 30 min (Figures 6C and 6D). To stringently evaluate KO effects on the LPS-dependent DC phosphoproteome, we focused on the 1,628 phosphosites mapping onto 990 unique proteins that were differentially regulated in both (1) LPS-treated wild-type DCs at 30–45 min (time course data; Table S1) and (2) $Myd88^{-/-}/Ticam1^{-/-}$ DCs compared to wild-type (Table S6). Out of these 1628 phosphosites, a third (38.1%, 621/1,628) were only affected by $Myd88^{-/-}/Ticam1^{-/-}$ double deletion, whereas the remaining sites were affected by both double and single mutants: 45.6% (742/1628) for $Irak4^{-/-}$, 31.1% (506/1628) for $Myd88^{-/-}$, and 8.1% (132/1,628) for $Irak2^{-/-}$. These numbers agree with the essential role of IRAK4 in TLR signaling (Picard et al., 2003; Suzuki et al., 2002) and the partially redundant function of IRAK2 with IRAK1 (Kawagoe et al., 2008). Furthermore, these 990 Myd88/Ticam1-dependent phosphoproteins captured 32.6% (46/141) of the canonical TLR proteins, including known phosphosites such as TBK1 S716 and JUN S63/S73 downregulated in $Myd88^{-/-}$ and $Irak4^{-/-}$ cells, IRF3

S379 impacted upon double KO only, or MAPK9 T183/Y185 by MYD88- and TRIF-dependent pathways (Figure S6B).

To complement this genetic approach, we developed a large-scale in vitro kinase (IVK) assay using recombinant kinases IRAK4, TBK1, and IRAK2 mixed with native protein lysates from SILAC-labeled DCs followed by phosphoproteomics (Figure 6E). We identified a total of 967 phosphosites upregulated by IRAK4, 325 by TBK1, and 201 by IRAK2, which included sites also upregulated in LPS-treated DCs: 55 out of 967 (5.7%) for IRAK4 and 62 out of 325 (19.1%) for TBK1 (Figures 6F, 6G, and S6C; Table S6). These results suggest that some of the phosphosites identified by IVK are likely to be physiologically relevant, although others might be due to off targets effects (e.g., activation of secondary kinases, or proximity with proteins in solution that would not exist in cells).

An Integrated Model Reveals Signaling-to-Transcription Paths across the TLR4 System

Lastly, we sought to combine our measurements on physical and functional interactions into an integrated model of signaling-to-transcription relationships in the TLR4 system (Figure S7A). We used a network-based approach that relies on three main steps (Figure 7A). First, we assembled a "background" network of 92,610 protein-protein and 5,533 kinase-substrate interactions from public repositories and 43 protein-protein and 230 kinase-substrate interactions identified from this study using DCs (Table S7). Second, we assigned weights to the edges
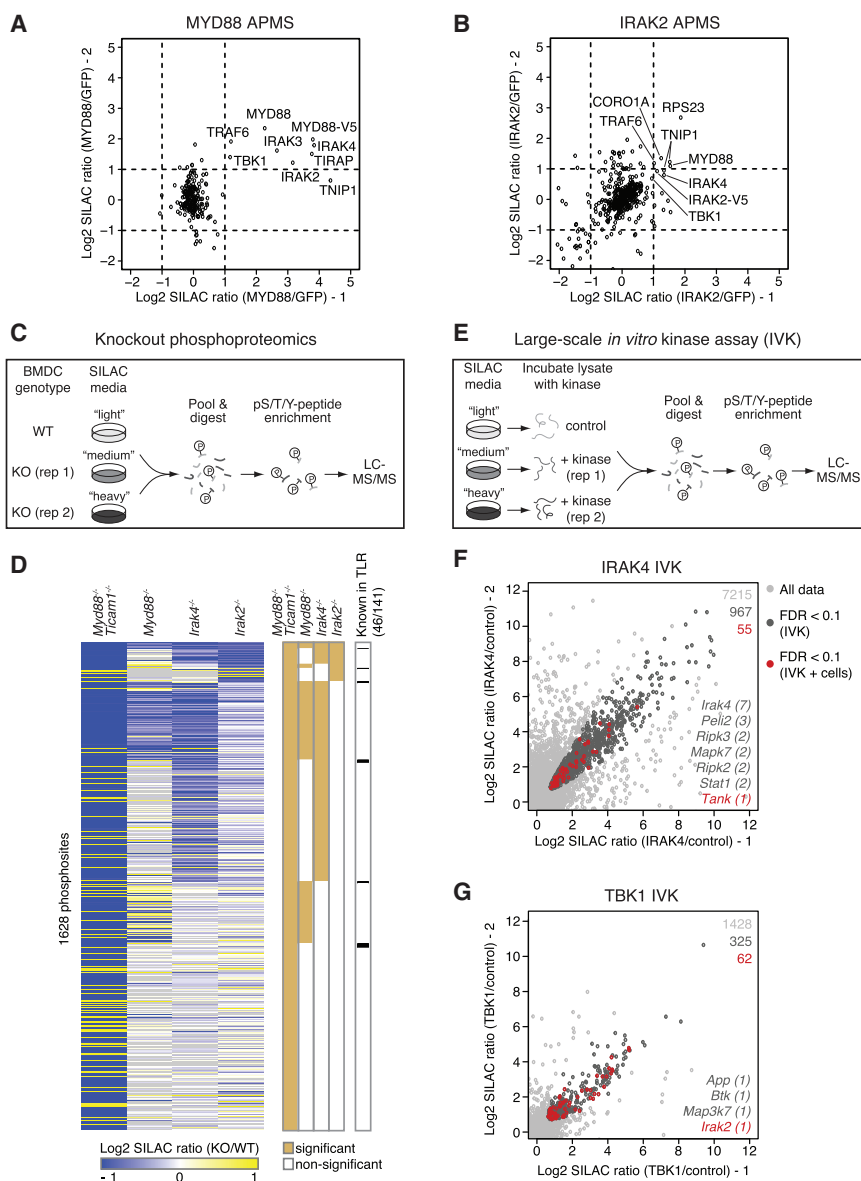
Figure 6. Physical and Functional Proteomics Assays Pinpoint Binding and Phosphorylation Events Downstream of the Myd88 Adaptor and Associated Kinases

(A and B) Affinity purification followed by proteomics. Shown are dot plots of SILAC ratios for proteins identified in DCs overexpressing V5-tagged MYD88 (A) or IRAK2 (B). Cells were stimulated with LPS for 30 min and protein complexes purified using anti-V5 antibodies coupled to magnetic beads. Each axis represents an independent experiment.

(C) Diagram depicting our experimental approach for measuring the impact of gene KO on the TLR4-regulated phosphoproteome of mouse BMDCs.

(D) Phosphoproteomics in KO cells. Left: heatmap for SILAC ratios of phosphosites (rows) in four KO models (columns) at 30 min after LPS stimulation compared to control wild-type cells, as indicated (gray, missing values). Middle: phosphosites with significant up- or downregulation in KO versus WT (light brown). Right: phosphosites belonging to known TLR proteins (black).

(E) Diagram depicting our experimental approach for large-scale in vitro kinase assays using native protein lysates from BMDCs and phosphoproteomics.

(F and G) In vitro kinase (IVK) assay followed by phosphoproteomics. Shown are scatterplots of SILAC ratios of phosphosites identified using the purified kinases IRAK4 (F) and TBK1 (G). Light gray, all data points; dark gray, phosphosites with FDR < 0.1 in IVK; red, phosphosites with FDR < 0.1 in both IVK and cells stimulated with LPS, which highlights the overlap between IVK and phosphoproteome measurements on stimulated cells (denoted as IVK + cells). Gene names at the bottom right of each plot indicate known TLR components with the number of phosphosites in parenthesis.

See also Figure S6 and Table S6.

(i.e., protein-protein and kinase-substrate interactions) and nodes (i.e., signaling or transcriptional regulators) of the background network to create a "weighted" interaction network based on the phosphorylation changes driven by LPS stimulation and specific kinases (based on KO and IVK data). Third, we searched the weighted network for biochemical paths linking the 29 phosphoproteins/signaling regulators or "seed nodes" to transcriptional regulators or "target nodes." To test the validity of this integrative algorithm, we quantified its performance in retrieving known seed-target relationships between canonical TLR pathway components using receiver-operator characteristic (ROC) curves. In the high precision regime, using a weighted network outperformed methods that used the background interaction network or phosphorylation data alone. For example, at a false positive rate (FPR) of 0.001, the weighted network method

yielded a true positive rate (TPR) that was 3.9 and 10.4 times higher than background network and "phosphorylation only" approaches, respectively (Figure S7B). Thus, our network-based approach correctly identified known signaling-to-transcription relationships between canonical TLR pathway components thanks to the information collected using DCs in this study.

Next, we searched for biochemical paths connecting the 29 signaling regulators highlighted above as "seeds" (Figure 5A) and the 782 TFs detected by mass spectrometry in bone marrow-derived dendritic cells (BMDCs) as "targets" (Table S1). We identified 420 significant relationships between 27 out of 29 seed(except for seed DMXL2 and RAB3IL1) and 95 out of 782 target nodes (p < 0.0005, FDR < 0.05), whereas only 12 relationships linking 7 seeds to 11 targets can be found without integrating our DC-specific datasets with publicly available interactions within our algorithmic framework (Figure 7B; Table S7). Each signaling node reached between 51 (TBK1) and 3 (ARHGEF11) TFs, for an
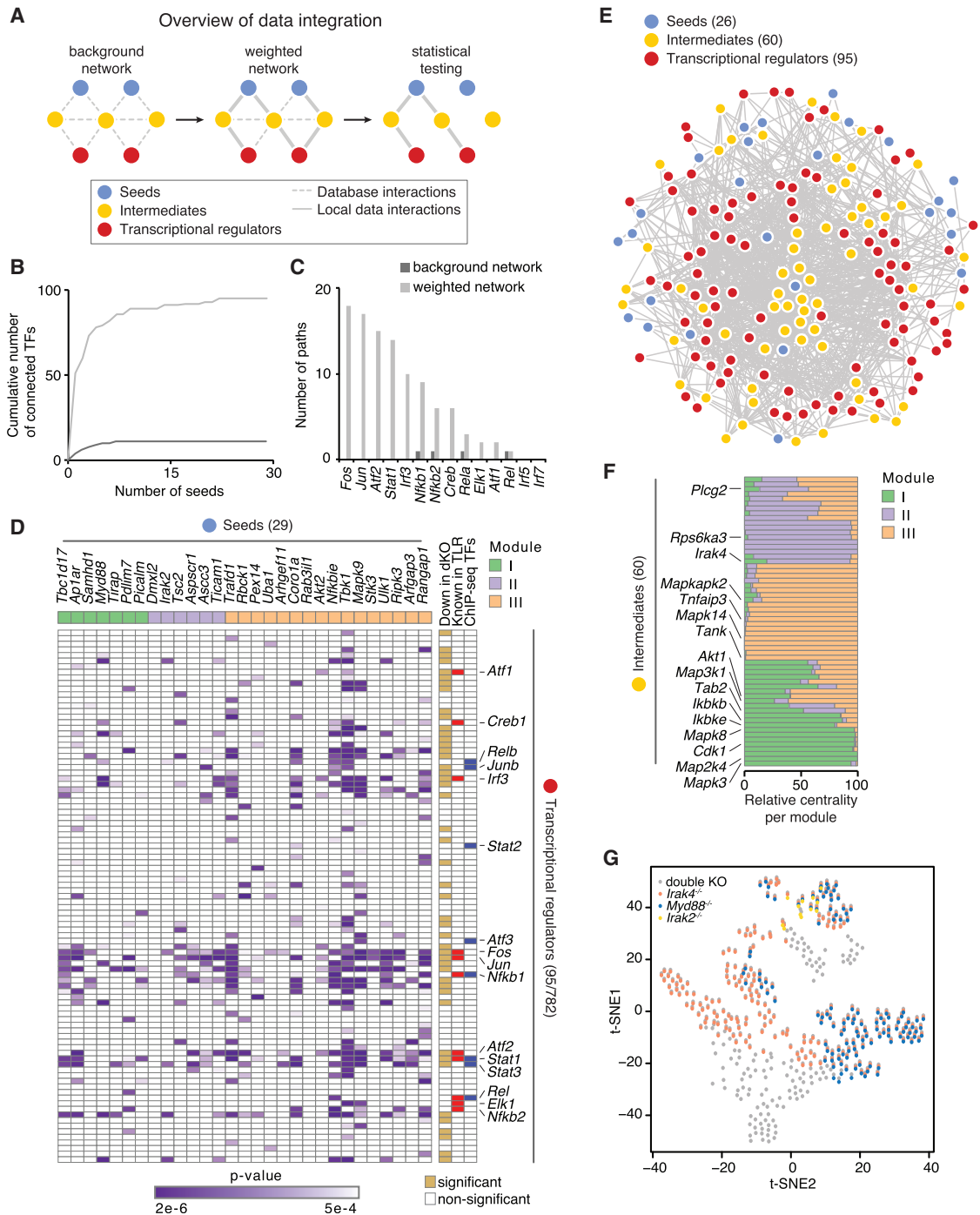
Figure 7. An Integrative Analysis Reveals Known and Candidate Signaling-to-Transcription Paths and Helps Parse the Effects of Myd88 and Associated Kinases in the TLR4 System

(A) A computational framework for integrative analysis of the functional and physical proteomics datasets collected in this study (from left to right). A background interaction network is assembled using database and local data, nodes and edges are scored based on experimental evidence from this work, and statistically significant relationships determined by bootstrap analysis.

(B) Cumulative number of significant relationships (bootstrap p value < 0.0005, FDR < 0.05) identified between seed nodes (29) and any of the transcriptional regulators detected in BMDCs (782 possible target nodes in total) using background network (dark gray) and weighted network (light gray) methods.

(C) Total number of relationships linking seeds (29) and known TLR transcription regulators (14) for background network (dark gray) and weighted network (light gray) methods.

(legend continued on next page)

average of 14.5 ± 11.6 SD. TFs via 1.5 ± 0.7 SD intermediate nodes (Figure S7C). Importantly, these signaling-to-transcription relationships captured 11 out of the 14 canonical TLR TFs and 8 out of 20 of the TFs whose binding sites were compared to knockdown effects (Figures 5B, 7C, and 7D). Furthermore, 49% (47/95) of the TFs were both upregulated at the phosphorylation level upon LPS stimulation and downregulated in $Myd88^{-/-}/Ticam1^{-/-}$ cells. Overall, each of the three modules identified based on co-phenotypes upon knockdown (Figure 5) appeared to be biochemically linked to similar downstream TFs (Figure 7D).

We asked which intermediate nodes were most central between seed and target nodes (i.e., most connected to target TF nodes). For the 420 significant relationships linking the 27 seed and 95 target nodes, we ranked the top 25 intermediates present across each of our three modules (Figure 7D), which lead to a total of 60 non-overlapping intermediate nodes that included 16 canonical TLR pathway components (Figures 7E and 7F). These 60 intermediate nodes displayed various levels of specificity across the three modules identified above, with for example IRAK4 being central to module II (i.e., connected to a relatively high number of nodes), whereas MAPK8 (JNK) and MAPK14 (P38) were more connected across modules I and III, respectively. Other nodes appeared shared between modules such as AKT1 for I and III or TAB2 for I, II, and III. Thus, intermediate nodes display both specific and shared roles across the regulatory modules of the TLR4 pathway, which likely reflects crosstalk within pathways leading to the regulation of overlapping sets of target genes.

To gain insights into how signal is distributed downstream of TLR4, we asked how the 420 seed-target relationships identified here were affected by the four KO strains used in this study (Figure 6D). We quantified how many of the nodes (seed, intermediate, and target) present in each of the 420 seed-target pairs were impacted at their phosphorylation level by KO. 391 out of the 420 pairs were significantly affected by $Myd88^{-/-}/Ticam1^{-/-}$, and 261 out of these 391 pairs were also impacted by $Myd88^{-/-}$, $Irak2^{-/-}$, and/or $Irak4^{-/-}$, leading to four clusters of effects: (1) double KO only or together with (2) IRAK4 alone, (3) IRAK4 and MYD88, or (4) IRAK4, MYD88, and IRAK2 (although to a lesser extent) (Figure 7G). Interestingly, a large fraction of TLR4 signals were impacted by MYD88 deletion, as expected, but IRAK4 was responsible for broader effects despite the presence of IRAK4 and MYD88 in the same complex. Seed-target pairs that were impacted by double-KO cells, but not MYD88 KO cells, are likely to be important for TRIF-dependent signaling (i.e., module II). Overall, this quantitative measurement of KO effects on signaling-to-transcription paths provides additional information on how signal is transmitted and partitioned from MYD88 and

some of its kinase partners to downstream signaling and transcriptional regulatory layers.

DISCUSSION

We established an integrative framework to dissect signal propagation in the TLR system using data spanning both signaling and transcriptional regulatory events. Previous studies have connected paths within networks largely using protein-protein interaction or phosphorylation data alone or in conjunction with one to two different types of experimental data (Gitter et al., 2013; Huang and Fraenkel, 2009; Huang et al., 2013; Terfve et al., 2015). This study provides a proof-of-principle example of the power of integrative analyses that take into account regulatory layers not typically studied in conjunction, from phosphorylation dynamics to relationships between kinases substrates to proteins forming complexes or binding to DNA to gene regulation. In future work, it will be crucial to take into account additional regulatory layers such as the spatial distribution of proteins (Brubaker et al., 2015), other PTMs and their enzymes (e.g., ubiquitination, acetylation) (Mertins et al., 2013), and post-transcriptional modifications (RNA) or translational control events.

The observations that AP1AR, its binding partner PICALM, and SAMHD1 might play a role in pro-inflammatory signaling will require future mechanistic studies. Interestingly, both AP1AR and its binding partner, PICALM, interact with clathrin adaptor proteins (Maritzen and Haucke, 2010; Miller et al., 2015), suggesting a link between the TLR4-MYD88 pathway and intracellular vesicle transport regulation that is reminiscent of the TLR4-TRIF axis (Kagan et al., 2008). In addition, previous work linked the $Ap1ar$ locus to TNF production by DCs triggering colitis (Ermann et al., 2011), which further support our results on the role of AP1AR in pro-inflammatory signaling. The other candidate regulator reported here, SAMHD1, is best characterized in viral restriction (Ballana and Esté, 2015), but it also plays a role in processes such as TNF-mediated pro-inflammatory signaling in fibroblasts (Liao et al., 2008), cell cycle (Pauls et al., 2014), or DNA damage (Clifford et al., 2014) and in disease such as AGS (Crow and Manel, 2015) and cancer (Schuh et al., 2012). LPS regulated both known and previously unrecognized phosphosites on SAMHD1 such as T634, mouse ortholog site for the known human T592 regulatory site targeted by CDK2 (Pauls et al., 2014), or T52 found in the poorly characterized SAM domain and that was regulated in a MYD88-dependent manner. Taken together, these observations provide valuable information for future mechanistic investigations.

The multi-layer datasets reported here will be useful for further analyses, mining and hypothesis-generating purposes

---

(D) Significant relationships (420 pairs) found between 29 seeds (columns) and 95 transcriptional regulators (rows). Modules from Figures 3B and 5A are shown (columns) in light green (I), purple (II), and orange (III). Transcriptional regulators with phosphosites with significant up- or downregulation in $Myd88^{-/-}/Ticam1^{-/-}$ versus WT and in time series are indicated on the right (light brown). P values, bootstrap (purple).

(E) An interaction network connects 27 seeds (blue) to 95 transcriptional regulators (red) through the top 60 intermediate (yellow) nodes that were ranked based on centrality measure (see Experimental Procedures).

(F) Centrality score of the top 60 intermediate nodes across the three modules from (D).

(G) t-distributed stochastic neighbor embedding (t-SNE) analysis of the effects of gene KO (data from Figure 6D) on the phosphorylation levels of nodes present in the paths mediating the seed-transcriptional regulator relationships identified in (D). Shown are all of the 391 out of 420 relationships affected by $Myd88^{-/-}/Ticam1^{-/-}$ (gray dots). The effects of Irak4, Myd88, and Irak2 on these paths are overlaid in orange, blue, and yellow, respectively.

See also Figure S7 and Table S7.

on additional candidate regulators, from the protein to the phosphosite level. First, many of the 131 phosphoproteins selected for genetic screening had little to no effect on gene expression. While poor knockdown efficiency and functional redundancy can likely explain some of these cases, measuring the effects of perturbing these proteins on other aspects of DC biology such as motility or antigen presentation might help uncover important mechanisms. Second, we focused our targeted screen for regulators of gene expression on enzymes and their regulators, but screening additional molecular functions is likely to uncover additional regulators. For example, 24 phosphoproteins downregulated between 180 and 240 min after LPS stimulation are involved in RNA binding and include the known pathogen-sensing regulators *Ddx21*, *Ddx3x*, or *Adar* and a host of potential candidates for this nascent area in TLR biology (Anderson, 2010).

Lastly, it will be critical to build upon this work to systematically identify functional phosphosites and their matching kinases. Our study correctly identified many phosphosites of canonical TLR components or other pathogen-sensing pathways such as NLRC4 S533, which is a key site for host immunity (Qu et al., 2012). Our large-scale IVK assay uncovered many known and candidate substrates that will be important to validate using in vivo chemical genetics approaches (Allen et al., 2007) and shorter timescales to increase confidence about substrate specificity as shown in bacteria and yeast (Kanshin et al., 2015; Skerker et al., 2008). Thus, future research on screening functional phosphosites using site-directed mutagenesis will help to reveal phosphorylated residues with functional significance and potential therapeutic value.

EXPERIMENTAL PROCEDURES

Cells
Bone-marrow-derived DCs were generated from 6- to 8-week-old female C57BL/6J (The Jackson Laboratory), $Ap1ar^{-/-}$ (Maritzen et al., 2012), $Samhd1^{-/-}$ (Rehwinkel et al., 2013), $Myd88^{-/-}$, $Myd88^{-/-}/Ticam^{-/-}$, $Irak2^{-/-}$, $Irak4^{-/-}$ mice. All stimulations were performed using ultra-pure *E. coli* K12 LPS (Invivogen) at 100 ng/mL. For shRNA knockdowns, high-titer lentiviruses expressing shRNAs were used to infect bone marrow cells as previously described (Chevrier et al., 2011).

mRNA Measurements
Total or poly(A)$^+$ RNA was extracted and reverse transcribed prior to qPCR analysis with SYBR green (Roche) in triplicate with *Gapdh* for normalization. For mRNA counting, 5×10^4 bone-marrow-derived DCs were lysed in RLT buffer (QIAGEN) with 1% β-ME (beta-mercaptoethanol). 10% of the lysate was used for mRNA counting using the nCounter Digital Analyzer (NanoString) and a custom CodeSet constructed to detect a total of 267 genes (including 16 control genes whose expression remain unaffected by TLR stimulation). To determine significantly affected signature genes, a fold-change ratio is computed for each pairwise comparison of a knockdown sample versus a set of control samples (i.e., non-targeting shRNA; at least ten per experimental batch).

Affinity Purification followed by Mass Spectrometry
Analysis of interaction partners of V5-tagged proteins (MYD88, IRAK2 and AP1AR) was performed using a single-step purification procedure as previously described (Hubner and Mann, 2011), with several modifications. Peptide samples were analyzed on a Q Exactive mass spectrometer (Thermo Fisher Scientific), and mass spectra were processed as described above.

Large-Scale Phosphoproteome and Proteome Analyses
For temporal phosphoproteome analysis, BMDCs grown in SILAC media were stimulated with LPS and lysed and processed for enrichment of phosphopeptides using strong cation exchange chromatography (SCX)/IMAC (immobilized metal affinity chromatography) as described previously (Chevrier et al., 2011). For IVK and KO phosphoproteome analysis, peptide samples were separated by basic reversed-phase (RP) prior to IMAC enrichment as described previously (Mertins et al., 2013). IVK reactions were performed with recombinant kinases for IRAK2, IRAK4, or TBK1 on SILAC-labeled native cell lysates from DCs. For proteome analysis, total peptides were separated into 12 fractions using an Agilent 3100 Offgel fractionator. Peptide samples were analyzed on LTQ Orbitrap, LTQ Orbitrap Velos, or Q Exactive mass spectrometer (Thermo Fisher Scientific). To identify and quantify peptides, mass spectra were processed with the Spectrum Mill (Agilent Technologies) and the MaxQuant (version 1.2.2.5) software packages (Cox and Mann, 2008). Details on differential expression, clustering, pathway enrichment, and network analyses are in the Supplemental Experimental Procedures.

ACCESSION NUMBERS

The accession number for the original mass spectra data reported in this paper is MassIVE : MSV000081071. The data are directly accessible via ftp:// massive.ucsd.edu/MSV000081071.

SUPPLEMENTAL INFORMATION

Supplemental Information includes Supplemental Experimental Procedures, seven figures, and seven tables and can be found with this article online at http://dx.doi.org/10.1016/j.celrep.2017.06.016.

AUTHOR CONTRIBUTIONS

N.C. designed the study and performed experiments; P.M. and J.Q. performed mass spectrometry; R.R. and T.M.E. contributed to experiments; D.P., P.M., N.Y., and N.C. performed computational analyses; T.M., V.H., T.S., and S.A. contributed knockout bone marrow cells; and P.M., D.P., S.A.C., A.R., N.H., and N.C. wrote the manuscript with input from all authors.

ACKNOWLEDGMENTS

REFERENCES

Allen, J.J., Li, M., Brinkworth, C.S., Paulson, J.L., Wang, D., Hübner, A., Chou, W.-H., Davis, R.J., Burlingame, A.L., Messing, R.O., et al. (2007). A semisynthetic epitope for kinase substrates. Nat. Methods *4*, 511–516.

Anderson, P. (2010). Post-transcriptional regulons coordinate the initiation and resolution of inflammation. Nat. Rev. Immunol. *10*, 24–35.

Ballana, E., and Esté, J.A. (2015). SAMHD1: at the crossroads of cell proliferation, immune responses, and virus restriction. Trends Microbiol. *23*, 680–692.

Bensimon, A., Heck, A.J.R., and Aebersold, R. (2012). Mass spectrometry-based proteomics and network biology. Annu. Rev. Biochem. *81*, 379–405.

Bodenmiller, B., Wanka, S., Kraft, C., Urban, J., Campbell, D., Pedrioli, P.G., Gerrits, B., Picotti, P., Lam, H., Vitek, O., et al. (2010). Phosphoproteomic analysis reveals interconnected system-wide responses to perturbations of kinases and phosphatases in yeast. Sci. Signal. 3, rs4.

Brubaker, S.W., Bonham, K.S., Zanoni, I., and Kagan, J.C. (2015). Innate immune pattern recognition: a cell biological perspective. Annu. Rev. Immunol. 33, 257–290.

Chevrier, N., Mertins, P., Artyomov, M.N., Shalek, A.K., Iannacone, M., Ciaccio, M.F., Gat-Viks, I., Tonti, E., DeGrace, M.M., Clauser, K.R., et al. (2011). Systematic discovery of TLR signaling components delineates viral-sensing circuits. Cell 147, 853–867.

Clifford, R., Louis, T., Robbe, P., Ackroyd, S., Burns, A., Timbs, A.T., Wright Colopy, G., Dreau, H., Sigaux, F., Judde, J.G., et al. (2014). SAMHD1 is mutated recurrently in chronic lymphocytic leukemia and is involved in response to DNA damage. Blood 123, 1021–1031.

Cox, J., and Mann, M. (2008). MaxQuant enables high peptide identification rates, individualized p.p.b.-range mass accuracies and proteome-wide protein quantification. Nat. Biotechnol. 26, 1367–1372.

Crow, Y.J., and Manel, N. (2015). Aicardi-Goutières syndrome and the type I interferonopathies. Nat. Rev. Immunol. 15, 429–440.

Eriksen, A.B., Torgersen, M.L., Holm, K.L., Abrahamsen, G., Spurkland, A., Moskaug, J.Ø., Simonsen, A., and Blomhoff, H.K. (2015). Retinoic acid-induced IgG production in TLR-activated human primary B cells involves ULK1-mediated autophagy. Autophagy 11, 460–471.

Ermann, J., Garrett, W.S., Kuchroo, J., Rourida, K., Glickman, J.N., Bleich, A., and Glimcher, L.H. (2011). Severity of innate immune-mediated colitis is controlled by the cytokine deficiency-induced colitis susceptibility-1 (Cdcs1) locus. Proc. Natl. Acad. Sci. USA 108, 7137–7141.

Garber, M., Yosef, N., Goren, A., Raychowdhury, R., Thielke, A., Guttman, M., Robinson, J., Minie, B., Chevrier, N., Itzhaki, Z., et al. (2012). A high-throughput chromatin immunoprecipitation approach reveals principles of dynamic gene regulation in mammals. Mol. Cell 47, 810–822.

Geng, J., Sun, X., Wang, P., Zhang, S., Wang, X., Wu, H., Hong, L., Xie, C., Li, X., Zhao, H., et al. (2015). Kinases Mst1 and Mst2 positively regulate phagocytic induction of reactive oxygen species and bactericidal activity. Nat. Immunol. 16, 1142–1152.

Gitter, A., Carmi, M., Barkai, N., and Bar-Joseph, Z. (2013). Linking the signaling cascades and dynamic regulatory networks controlling stress responses. Genome Res. 23, 365–376.

Hasan, U.A., Caux, C., Perrot, I., Doffin, A.-C., Menetrier-Caux, C., Trinchieri, G., Tommasino, M., and Vlach, J. (2007). Cell proliferation and survival induced by Toll-like receptors is antagonized by type I IFNs. Proc. Natl. Acad. Sci. USA 104, 8047–8052.

Huang, S.-S.C., and Fraenkel, E. (2009). Integrating proteomic, transcriptional, and interactome data reveals hidden components of signaling and regulatory networks. Sci. Signal. 2, ra40.

Huang, S.-S.C., Clarke, D.C., Gosline, S.J.C., Labadorf, A., Chouinard, C.R., Gordon, W., Lauffenburger, D.A., and Fraenkel, E. (2013). Linking proteomic and transcriptional data through the interactome and epigenome reveals a map of oncogene-induced signaling. PLoS Comput. Biol. 9, e1002887.

Hubner, N.C., and Mann, M. (2011). Extracting gene function from protein-protein interactions using Quantitative BAC InteraCtomics (QUBIC). Methods 53, 453–459.

Huttlin, E.L., Ting, L., Bruckner, R.J., Gebreab, F., Gygi, M.P., Szpyt, J., Tam, S., Zarraga, G., Colby, G., Baltier, K., et al. (2015). The BioPlex network: a systematic exploration of the human interactome. Cell 162, 425–440.

Kagan, J.C., Su, T., Horng, T., Chow, A., Akira, S., and Medzhitov, R. (2008). TRAM couples endocytosis of Toll-like receptor 4 to the induction of interferon-beta. Nat. Immunol. 9, 361–368.

Kanshin, E., Bergeron-Sandoval, L.-P., Isik, S.S., Thibault, P., and Michnick, S.W. (2015). A cell-signaling network temporally resolves specific versus promiscuous phosphorylation. Cell Rep. 10, 1202–1214.

Kawagoe, T., Sato, S., Matsushita, K., Kato, H., Matsui, K., Kumagai, Y., Saitoh, T., Kawai, T., Takeuchi, O., and Akira, S. (2008). Sequential control of Toll-like receptor-dependent responses by IRAK1 and IRAK2. Nat. Immunol. 9, 684–691.

Li, S., Wang, L., Berman, M., Kong, Y.-Y., and Dorf, M.E. (2011). Mapping a dynamic innate immunity protein interaction network regulating type I interferon production. Immunity 35, 426–440.

Liao, W., Bao, Z., Cheng, C., Mok, Y.-K., and Wong, W.S.F. (2008). Dendritic cell-derived interferon-γ-induced protein mediates tumor necrosis factor-α stimulation of human lung fibroblasts. Proteomics 8, 2640–2650.

Maritzen, T., and Haucke, V. (2010). Gadkin: A novel link between endosomal vesicles and microtubule tracks. Commun. Integr. Biol. 3, 299–302.

Maritzen, T., Zech, T., Schmidt, M.R., Krause, E., Machesky, L.M., and Haucke, V. (2012). Gadkin negatively regulates cell spreading and motility via sequestration of the actin-nucleating ARP2/3 complex. Proc. Natl. Acad. Sci. USA 109, 10382–10387.

Mertins, P., Qiao, J.W., Patel, J., Udeshi, N.D., Clauser, K.R., Mani, D.R., Burgess, M.W., Gillette, M.A., Jaffe, J.D., and Carr, S.A. (2013). Integrated proteomic analysis of post-translational modifications by serial enrichment. Nat. Methods 10, 634–637.

Miller, S.E., Mathiasen, S., Bright, N.A., Pierre, F., Kelly, B.T., Kladt, N., Schauss, A., Merrifield, C.J., Stamou, D., Höning, S., and Owen, D.J. (2015). CALM regulates clathrin-coated vesicle size and maturation by directly sensing and driving membrane curvature. Dev. Cell 33, 163–175.

Pauls, E., Ruiz, A., Badia, R., Permanyer, M., Gubern, A., Riveira-Muñoz, E., Torres-Torronteras, J., Álvarez, M., Mothe, B., Brander, C., et al. (2014). Cell cycle control and HIV-1 susceptibility are linked by CDK6-dependent CDK2 phosphorylation of SAMHD1 in myeloid and lymphoid cells. J. Immunol. 193, 1988–1997.

Picard, C., Puel, A., Bonnet, M., Ku, C.-L., Bustamante, J., Yang, K., Soudais, C., Dupuis, S., Feinberg, J., Fieschi, C., et al. (2003). Pyogenic bacterial infections in humans with IRAK-4 deficiency. Science 299, 2076–2079.

Qu, Y., Misaghi, S., Izrael-Tomasevic, A., Newton, K., Gilmour, L.L., Lamkanfi, M., Louie, S., Kayagaki, N., Liu, J., Kömüves, L., et al. (2012). Phosphorylation of NLRC4 is critical for inflammasome activation. Nature 490, 539–542.

Rehwinkel, J., Maelfait, J., Bridgeman, A., Rigby, R., Hayward, B., Liberatore, R.A., Bieniasz, P.D., Towers, G.J., Moita, L.F., Crow, Y.J., et al. (2013). SAMHD1-dependent retroviral control and escape in mice. EMBO J. 32, 2454–2462.

Sanada, T., Takaesu, G., Mashima, R., Yoshida, R., Kobayashi, T., and Yoshimura, A. (2008). FLN29 deficiency reveals its negative regulatory role in the Toll-like receptor (TLR) and retinoic acid-inducible gene I (RIG-I)-like helicase signaling pathway. J. Biol. Chem. 283, 33858–33864.

Santra, T., Kolch, W., and Kholodenko, B.N. (2014). Navigating the multilayered organization of eukaryotic signaling: a new trend in data integration. PLoS Comput. Biol. 10, e1003385.

Schuh, A., Becq, J., Humphray, S., Alexa, A., Burns, A., Clifford, R., Feller, S.M., Grocock, R., Henderson, S., Khrebtukova, I., et al. (2012). Monitoring chronic lymphocytic leukemia progression by whole genome sequencing reveals heterogeneous clonal evolution patterns. Blood 120, 4191–4196.

Sharma, K., Kumar, C., Kéri, G., Breitkopf, S.B., Oppermann, F.S., and Daub, H. (2010). Quantitative analysis of kinase-proximal signaling in lipopolysaccharide-induced innate immune response. J. Proteome Res. 9, 2539–2549.

Sjoelund, V., Smelkinson, M., and Nita-Lazar, A. (2014). Phosphoproteome profiling of the macrophage response to different toll-like receptor ligands identifies differences in global phosphorylation dynamics. J. Proteome Res. 13, 5185–5197.

Skerker, J.M., Perchuk, B.S., Siryaporn, A., Lubin, E.A., Ashenberg, O., Goulian, M., and Laub, M.T. (2008). Rewiring the specificity of two-component signal transduction systems. Cell 133, 1043–1054.

Suzuki, N., Suzuki, S., Duncan, G.S., Millar, D.G., Wada, T., Mirtsos, C., Takada, H., Wakeham, A., Itie, A., Li, S., et al. (2002). Severe impairment of interleukin-1 and Toll-like receptor signalling in mice lacking IRAK-4. Nature *416*, 750–756.

Takeuchi, O., and Akira, S. (2010). Pattern recognition receptors and inflammation. Cell *140*, 805–820.

Tanigawa, K., Suzuki, K., Kimura, H., Takeshita, F., Wu, H., Akama, T., Kawashima, A., and Ishii, N. (2009). Tryptophan aspartate-containing coat protein (CORO1A) suppresses Toll-like receptor signalling in Mycobacterium leprae infection. Clin. Exp. Immunol. *156*, 495–501.

Terfve, C.D.A., Wilkes, E.H., Casado, P., Cutillas, P.R., and Saez-Rodriguez, J. (2015). Large-scale models of signal propagation in human cells derived from discovery phosphoproteomic data. Nat. Commun. *6*, 8033.

Weintz, G., Olsen, J.V., Frühauf, K., Niedzielska, M., Amit, I., Jantsch, J., Mages, J., Frech, C., Dölken, L., Mann, M., and Lang, R. (2010). The phosphoproteome of toll-like receptor-activated macrophages. Mol. Syst. Biol. *6*, 371.

Yugi, K., Kubota, H., Hatano, A., and Kuroda, S. (2016). Trans-Omics: how to reconstruct biochemical networks across multiple 'omic' layers. Trends Biotechnol. *34*, 276–290.